Available online at www.sciencedirect.com

ScienceDirect

Advances in Space Research 57 (2016) 919–927

ADVANCES IN SPACE RESEARCH (a COSPAR publication)

www.elsevier.com/locate/asr

Abundance and distribution of radioelements in lunar terranes: Results of Chang'E-1 gamma ray spectrometer data

Jian Chen [a], Zongcheng Ling [a,b,*], Bo Li [a], Jiang Zhang [a], Lingzhi Sun [a], Jianzhong Liu [c]

[a] Shandong Provincial Key Laboratory of Optical Astronomy and Solar-Terrestrial Environment, Institute of Space Sciences, Shandong University, 180 Wenhua Xilu, Weihai 264209, China

[b] Key Laboratory of Lunar and Deep Space Exploration, Chinese Academy of Sciences, 20 Datunlujia, Beijing 100012, China

[c] Institute of Geochemistry, Chinese Academy of Sciences, 46 Guanshui Road, Guiyang, Guizhou 550002, China

Received 7 June 2015; received in revised form 20 October 2015; accepted 20 November 2015
Available online 27 November 2015

Abstract

The gamma ray spectrometer (GRS) onboard Chang'E-1 has acquired valuable datasets recording the gamma ray intensities from radioelements (Potassium (K), Thorium (Th) and Uranium (U), etc.) on lunar surface. We extracted the elemental concentrations from the GRS data with spectral fitting techniques and mapped the global absolute abundance of radioelements in terms of the ground truths from lunar samples and meteorites. The obtained global concentration maps of these radioelements indicate heterogeneous distribution among three major lunar crustal terranes (i.e., Procellarum KREEP Terrane (PKT), Feldspathic Highlands Terrane (FHT), and South Pole Aitken Terrane (SPAT)) in relation with their origin and distinct geologic history. The majority of radioelements are restricted in PKT, approving the scenario of KREEP (Potassium (K), rare earth elements (REE), Phosphorus (P)) residua concentrating under the Procellarum region. Moreover, we found the consistency of distribution for radioelements and basalts, concluding that the subsequent volcanism might be associated with local concentrations of radioelements in western Oceanus Procellarum and northwestern South Pole Aitken Basin. The prominent and asymmetric radioactive signatures were confirmed in SPAT comparing to FHT dominated by low level radioactivity, while the magnitudes are much lower than that of PKT, indicating a primary geochemical heterogeneity for the Moon.

Keywords: Chang'E-1 GRS; Radioelements; Spectral fitting; Lunar terranes; Magmatic processes

1. Introduction

Lunar radioelements are enriched in materials composed by incompatible elements, which are also named as KREEP (Potassium (K), rare earth elements (REE), Phosphorus (P)) materials. According to the concept of Lunar Magma Ocean (LMO), KREEP materials formed as residue in the last stage of LMO due to their difficulty of crystallization, and deposited on crust–mantle boundary layer of the Moon (Warren, 1985). KREEP materials were emplaced on lunar surface via various geologic processes such as impact and volcanic eruption, etc. Consequently, spatial distribution of KREEP or radioelements near lunar surface is an important indication of the geologic processes and evolution of the Moon.

Previous lunar explorations have already proved that gamma ray spectroscopy is powerful to derive absolute abundances of radioelements. The GRS aboard Apollo 15 and 16 were two pioneers, which succeeded to portray concentrations of Th and K for ~60 lunar regions

* Corresponding author at: Shandong Provincial Key Laboratory of Optical Astronomy and Solar-Terrestrial Environment, Institute of Space Sciences, Shandong University, 180 Wenhua Xilu, Weihai 264209, China.
E-mail addresses: cjaxy2012@163.com (J. Chen), zcling@sdu.edu.cn (Z. Ling), libralibo@sdu.edu.cn (B. Li), zhang_jiang@sdu.edu.cn (J. Zhang), sunlz@mail.sdu.edu.cn (L. Sun), liujz@nao.cas.cn (J. Liu).

http://dx.doi.org/10.1016/j.asr.2015.11.018
0273-1177/

(Harrington et al., 1974; Bielefeld et al., 1976). The first global gamma ray spectroscopic measurement was carried out by Lunar Prospector (LP) (Feldman et al., 2004). Distribution of Th, K and U (rely on Th) has been determined from data obtained by LP GRS (Prettyman et al., 2006). Recently, Th and K maps were obtained by Kaguya GRS (KGRS) with higher sensitivity and precision (Hasebe et al., 2008; Kobayashi et al., 2010, 2012), and the lunar U distribution was directly derived by KGRS for the first time (Yamashita et al., 2010).

Chang'E-1 also achieved orbital observations of GRS, which employed CsI (Tl) scintillator as major detector (Ma et al., 2008). Lunar gamma ray spectra within energy region between 0.3 and 10 MeV were recorded by Chang'E-1 GRS (CGRS). The spectral resolution of CGRS is 8.3%@662 keV in the ground calibration (Ma et al., 2008) and 16.05%@511 keV in the lunar orbit (Zou et al., 2011), respectively. CGRS executed orbital measurements of lunar surface for about eight months (i.e., beginning from November 27, 2007, ending at July 25, 2008) on the altitude of ~200 km (Zhu et al., 2010). According to the proportional relationship between spatial footprint and orbital altitude for lunar gamma ray remote sensing, the spatial resolution of CGRS is ~300 km (about 1.5 times of the height above lunar surface (Lawrence et al., 2003)).

Massive amounts of data acquired by CGRS provide a good opportunity for us to recognize and understand global distribution of radioelements on lunar surface. While majority of elemental peaks in CGRS spectra are interfered by each other due to limited spectral resolution. Zhu et al. (2010, 2011) and Zou et al. (2011) have reported preliminary radioelements maps utilizing energy band methods. In this paper, based on the level 2C scientific data of GRS datasets of Chang'E-1, we have carried out spectral fitting to derive the contribution of radioelements in overlapping peaks. Then, the absolute abundances were calibrated according to returned lunar soil samples as well as feldspathic meteorites. We mapped the global distribution of radioelements, with intent to explore the potential of CGRS data in the understanding of lunar geochemical and thermal evolution history.

2. Methodology

CGRS level 2C data, distributed by the Ground Research and Application System (GRAS) of Chang'E-1 Program, have undergone a series of processing pipelines including gain correction, dead time correction, geometric correction, and orbit altitude normalization, etc. (Zhang et al., 2011). Our processing procedures (shown in Fig. 1) for level 2C data are as follows.

2.1. Data selections

Although the preprocessing procedures have been done, that still leave incorrect data (e.g., spectra with anomalously high values) caused by spatial environment

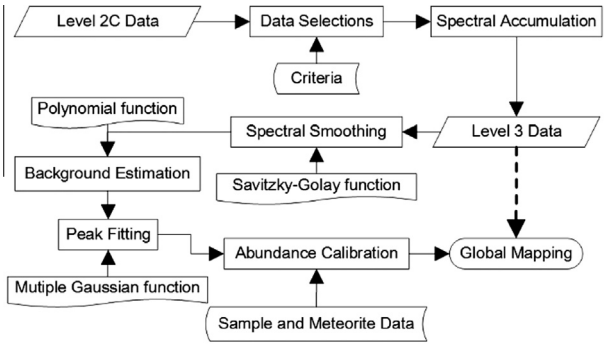

Fig. 1. Processing procedures of CGRS level 2C data.

variations and abnormal states of CGRS within level 2C datasets. Therefore data selections were carried out for level 2C data, in order to guarantee accuracy of elemental results in this work. Empirically, high voltage level, quality status and overall counts were chosen as three criteria for data selections (Zhang et al., 2011).

2.2. Spectral accumulation and smoothing

Due to the randomness of nuclear reactions, statistical fluctuations become an unavoidable factor to influence counts of gamma ray spectra. We tried to suppress statistical fluctuations by means of spectral summing in large pixels, which is reasonable in consideration of large spatial footprint for the uncollimated, omnidirectional instrument (Lawrence et al., 2004). In this work, all of spectra measured during the whole observation were accumulated in approximately equal area pixels on lunar surface. Meanwhile, data uncertainties were quantified by measuring the standard deviations of spectral counts in each pixel using Eq. (1) (Lawrence et al., 2004):

$$\sigma = \sqrt{\frac{\sum_{i=0}^{N_{spectra}} (S_i - S)^2}{N_{spectra} - 1}} \quad (1)$$

where σ is the standard deviation, $N_{spectra}$ is the number of spectra accumulated in each pixel, S_i is the counts of selected energy regions in each spectrum, and S is the mean counts in each pixel. Based on Eq. (1), we have acquired relative uncertainties (σ/S) of three energy regions corresponding to radioelements peaks listed in Table 1. In addition, we adopted a Savitzky–Golay function to smooth the spectra with intent to optimize the signal to background ratio of elemental peaks.

The accumulated spectrum of south pole region (poleward of 87.5°S) is shown in Fig. 2 as an example of CGRS level 3 data. Several recognizable peaks (Single escape peak@511 keV, Th@583, 2615 keV, U@609 keV, Mg@1368 keV, K@1461 keV and O@6129 keV) are labeled. The sharp increase in the low-energy edge of O peak was possibly incorrect channel counts caused by electronic error of the instrument. Nevertheless, the energy

Table 1
Energy regions of interest in our work along with their relative uncertainties of spectral counts and minimum count rate pixels.

Index	Energy region (keV)	Relative uncertainties (%)	Pixel with the minimum counts
I	464–669	7.91 ± 0.54	2.5–7.5°S, 150–55°W
II	1234–1719	8.31 ± 0.37	2.5–7.5°S, 150–155°W
III	2325–2888	12.26 ± 0.46	17.5–22.5°N, 150–155°W

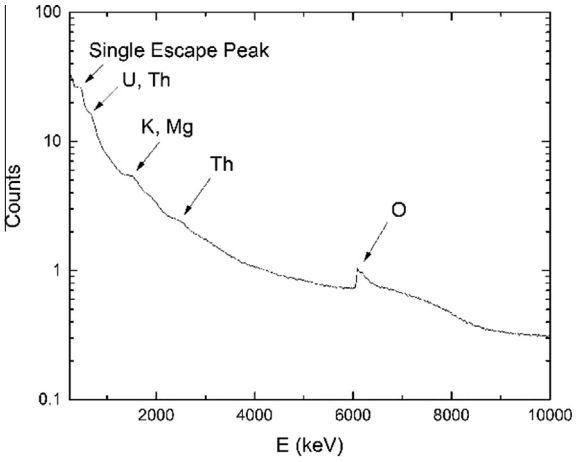

Fig. 2. CGRS spectra labeled by peaks of interest.

regions (~400–3000 keV) analyzed in this paper are far away from the discontinuity as well as its influence.

2.3. Background and peak fitting

Quantitative analyses of radioelements are based on the peak areas of individual elements from the GRS spectra. As seen from Fig. 2, peaks of radioelements are located above high background continuum so that measurements of elemental peak areas are evidently affected by the background counts. Therefore, background estimation is crucial to distinguish elemental peaks from the continuum. According to former detections of radioelements near lunar surface (LP GRS data from http://pds-geosciences.wustl.edu/missions/lunarp/reduced_special.html), the concentrations of radioelements are in close proximity to zero in certain regions of lunar highlands, where are thought to have the minimum count rate of radioelements (Lawrence et al., 2000). Consequently, spectra observed at the aforementioned pixels (see Table 1) were chosen for background fitting.

Other than background contribution, analyses of radioelements peaks are complicated by the highly overlapped peaks due to limited spectral resolution of CGRS. Energy region I recording gamma ray signals with the least uncertainties is dominated by ^{214}Bi line in ^{238}U decay chain@609 keV and single escape peak@511 keV, and contains considerable contribution from ^{208}Tl in ^{232}Th decay chain@583 keV under the two strongest peaks (Fig. 3a and d). Next, ^{40}K decay line@1461 keV coupled with ^{24}Mg (n, n' γ) peak@1368 keV makes up the composite peak in energy region II, whose uncertainties are slightly worse than energy region I (Fig. 3b and e). Other than 583 keV, another gamma ray line@2615 keV from ^{208}Tl is more independently identified in energy region III (Fig. 3c and f). Local spectral fitting for three energy regions were carried out using multiple Gaussian functions with polynomial backgrounds as shown in Fig. 3.

2.4. Calibration

The peak areas of radioelements in gamma ray spectra were calibrated to absolute concentrations by a linear fitting procedure utilizing chemical abundances of lunar soil samples (Haskin and Warren, 1991; Jolliff et al., 2006; Papike et al., 1998). Although there is difference in spatial resolutions between CGRS data (~300 km) and lunar samples (less than several kilometers around the landing sites), the soil and regolith samples could be suitable to reflect uniform chemical representatives in large spatial size comparing to remote sensing data because of continuous crater impacting (Gillis et al., 2004). However, there is no available data in lunar samples for southern nearside and northern farside highlands where are defined as FHT by Jolliff et al. (2000). Korotev et al. (2003) presented mean composition of feldspathic lunar meteorites (FLM) that offered us the best estimation of surface composition in FHT since these meteorites are thought as a random and average sampling of lunar feldspathic highlands. Our calibration model also included the FLM to constrain the results of FHT.

3. Results and discussion

Based on the linear fitting functions (Fig. 4), we derived the global distribution of radioelements on lunar surface using CGRS data (as shown in Fig. 5). The accuracy of CGRS radioelements maps depends on calibration, spectral fitting and intrinsic data uncertainties (see Table 1). Relative uncertainties of spectral fitting and calibration could be expressed as root mean squared error divided by fitting value. Average relative uncertainties of Th (583 keV), U, K and Th(2615 keV) peak areas acquired by spectral fitting are 0.22%, 0.35%, 0.04% and 0.04%. Likewise, corresponding calibration uncertainties are 3.06%, 3.63%, 1.33% and 9.43%, respectively. We produced two Th maps with the purpose of checking the reliability of derived Th distribution. However, the lower peak area and larger uncertainties of energy region III prevent a comparable result of Th distribution with that of energy region I. As indicated by Fig. 5d, regions with low 2615 keV Th peak area have been obscured and there are also less variations

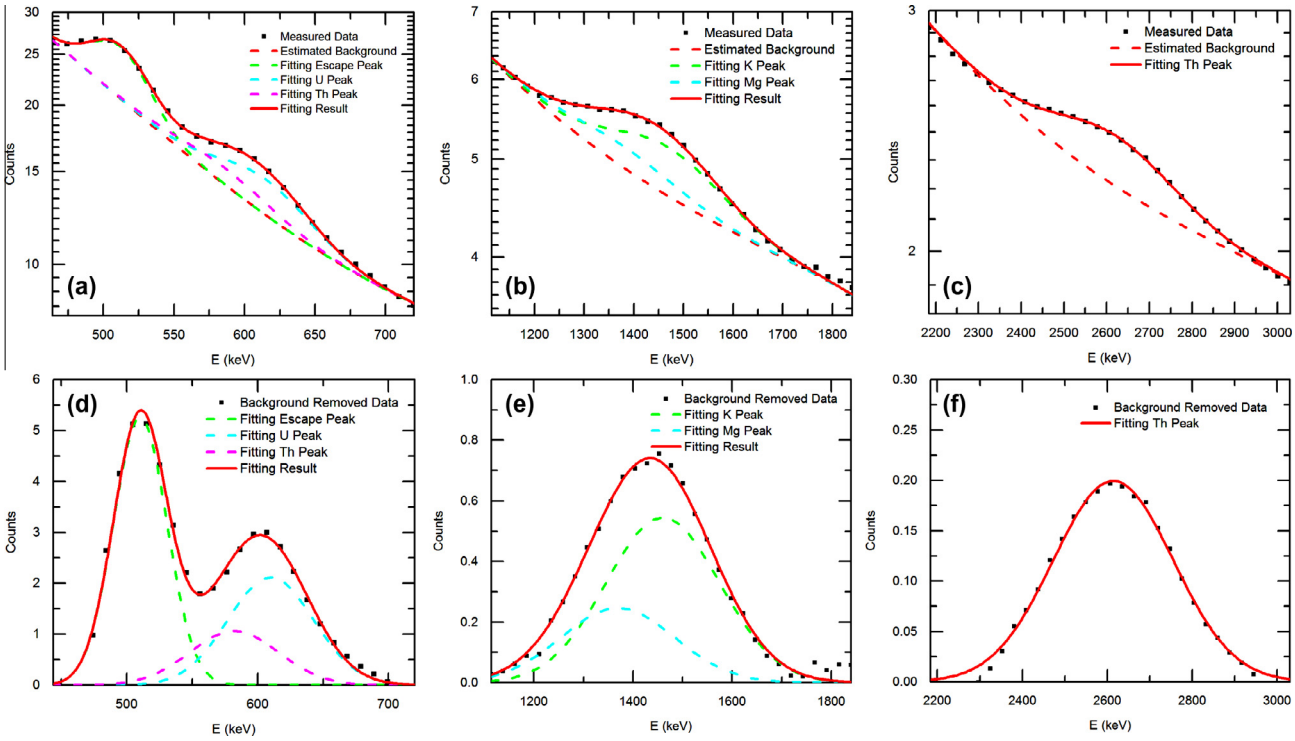

Fig. 3. Local spectral fitting diagrams of three energy regions.

in regions of high 2615 keV Th peak area (e.g., Surroundings of Imbrium). Th map derived from 2615 keV peak could be less reliable than that from 583 keV peak. Therefore, the result derived from 583 keV peak (Fig. 5a) is regarded as the true Th map in following discussion. To compare CGRS radioelements maps with previous study of radioelements abundances, we outlined PKT (Fig. 6) according to the contours of CGRS Th map (Th is chosen for discussion because of its better accuracy than K and U) and SPAT according to Chang'E-1 Digital Elevation Model (DEM) (Fig. 7), and then the rest was defined as FHT. The values in PKT, SPAT and FHT of CGRS results are all lower than former interpretations of LP GRS (see Table 2). It's reasonable considering the larger spatial resolution of CGRS (~300 km) than LP GRS (~150 km and ~45 km) that broader perspective would cover larger surface area around the peak point and thus weaken the average concentrations seen by orbiters. However, CGRS radioelements maps show higher peak values than KGRS (6.7 ppm Th and 2753 ppm K in Kobayashi et al. (2010); 7.3 ppm Th and 2.1 ppm U in Yamashita et al. (2010)) although the latter has lower orbital altitude (100 km, Hasebe et al., 2008) and higher spatial resolution. This may be attributed to the larger pixel size (450 km in Kobayashi et al. (2010); 9° in Yamashita et al. (2010)) of spectral accumulation used for KGRS maps.

According to CGRS global maps (Fig. 5), lunar radioelements are most concentrated in PKT and moderate enrichment in SPAT, while FHT is depleted of radioelements. Hence, following discussion will be also based on these typical geochemical provinces.

3.1. PKT

Several regions (e.g., Montes Jura, Apennine Bench, etc.; see Fig. 6) around Imbrium possess high abundances of radioactive components (~7–8.95 ppm Th). The oval pattern provides an implication that history of Imbrium region should be responsible to the distinct feature (Lawrence et al., 2000). Imbrium impact event was expected to have excavated substantial KREEP-rich materials covering regions around the basin (Haskin et al., 1998), whereas radioactivity inside Mare Imbrium was weakened by mare basalts filling since Upper Imbrium Epoch (beginning from ~3.8 Ga (Jolliff et al., 2006)). Furthermore, radioelements are much more emplaced at the southern side of Imbrium (~8–11.0 ppm Th) than the northern side (~3–7 ppm Th) that reveals possibly additional sources for the high radioactivity of PKT.

Contrary to Imbrium, the origin of Procellarum is still ambiguous. It was once interpreted as an ancient impact basin (Wilhelms et al., 1987), yet there isn't an obvious basin structure for Procellarum in topography (Smith et al., 2010). Neither circular nor elliptical shape of the western edge of Procellarum seems more likely to yield a nonimpact origin (Andrews-Hanna et al., 2014). The radioelements maps appear to support this speculation since high concentrations of radioelements present a pattern of surrounding Imbrium rather than hypothetical "Procellarum basin". A model has been proposed that KREEP-rich magma accumulated under the crust of Procellarum region (Jolliff et al., 2006). If that's indeed the case, radioactive components concentrated beneath

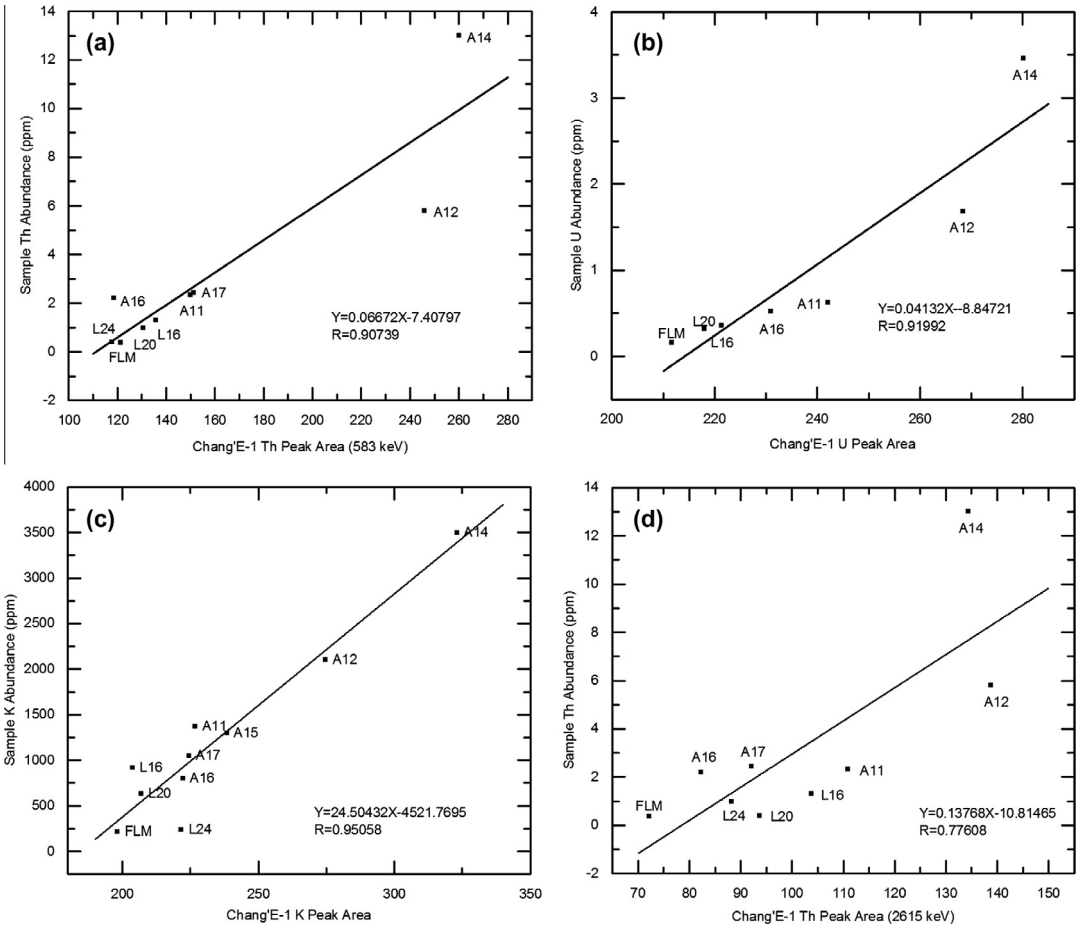

Fig. 4. Scatter plots of radioelements abundances in Apollo (A) and Luna (L) samples and feldspathic lunar meteorites (FLM) versus CGRS peak areas. Results of linear fitting are shown as regression lines, expressions and linear coefficients.

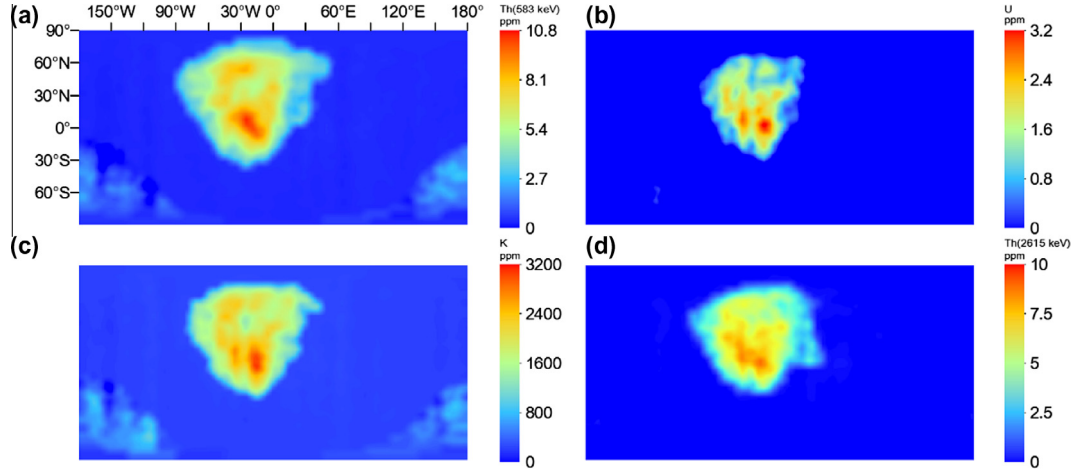

Fig. 5. Lunar radioelements ((a) Th (583 keV); (b) U; (c) K; (d) Th (2615 keV)) maps derived from CGRS data. Maps are smoothed in a circle neighborhood with a diameter of 300 km.

the Procellarum region, then Imbrium impact penetrated through local thin crust (Wieczorek et al., 2013) and induced subsequent large scale basalt eruptions (Jolliff et al., 2006) with possible emergence of radioelements in PKT.

Volcanic complexes confirmed in the Oceanus Procellarum show intense volcanic activities during the geologic history of PKT (Wilhelms et al., 1987). The radioactivity within PKT observed by CGRS would be either vertical mixing of basalt deposits and KREEP materials below or

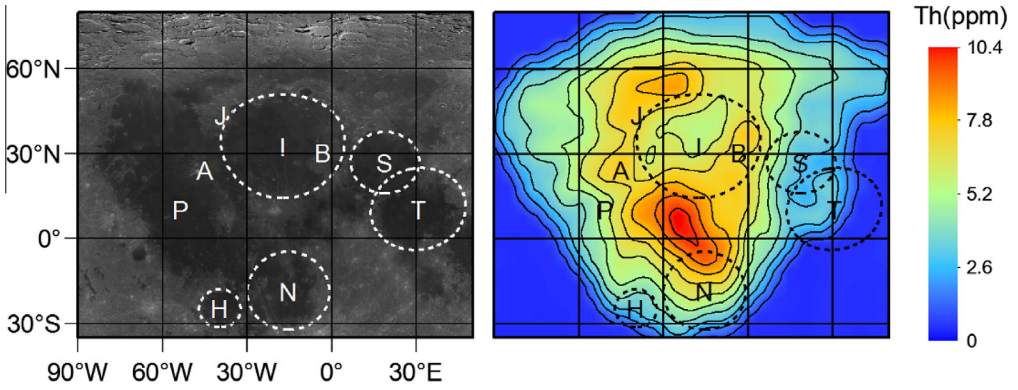

Fig. 6. Chang'E-1 CCD images and smoothed Th map with contours for PKT. Lunar nomenclatures mentioned in discussion have been labeled above, I = Imbrium, J = Montes Jura, B = Apennine Bench, P = Procellarum, A = Aristarchus, S = Serenitatis, H = Humorum, N = Nubium, T = Tranquillitatis.

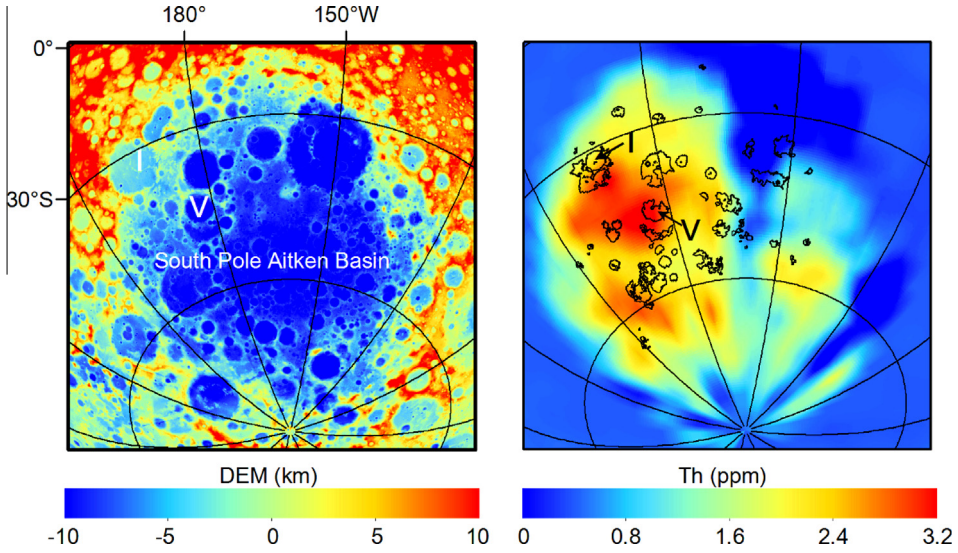

Fig. 7. Chang'E-1 Digital Elevation Model (DEM) and smoothed Th map in SPA. Mare regions within SPA are outlined, I = Mare Ingenii and V = Mare Von Kármán.

Table 2
Comparisons between CGRS results and LP GRS released data (from http://pds-geosciences.wustl.edu/missions/lunarp/reduced_special.html).

Terrane	Element	CGRS (ppm)	LP GRS (ppm)
Maximum in PKT	Th	11.0 ± 0.81	12.9 ± 0.34
	K	3393 ± 270	3991 ± 115
	U	3.37 ± 0.26	3.77 ± 0.09
Maximum in SPAT	Th	3.39 ± 0.28	4.9 ± 0.11
	K	1009 ± 83	1716 ± 99
	U	0.59 ± 0.05	1.2 ± 0.09
Average in FHT	Th	0.84 ± 0.07	1.56 ± 0.09
	K	374 ± 31	432 ± 77
	U	0.14 ± 0.01	0.31 ± 0.07

KREEP-bearing basalts as sampled by Apollo missions (Jolliff et al., 2006). No matter how it worked, the consistency between the boundaries of PKT determined by radioelements distribution and major basalt filled area, especially the western shoreline of Oceanus Procellarum (see Fig. 6) suggests possible correlation between these two phenomena (Haskin et al., 2000) that perhaps basaltic lava flows have played a crucial role in the emplacement of KREEP materials in PKT. Reciprocally, heat release from decay of radioelements would also contribute to magmatic evolution and volcanic processes. If local concentrations of radioelements originated from early period of lunar history, thermal evolution of PKT would be led by radioelements (Wieczorek and Phillips, 2000).

Another radioactive anomaly (~8–8.15 ppm Th) corresponds to Aristarchus region where is marked by high albedo of Copernican crater materials, widespread rilles and pyroclastic deposits on the northwestern highlands (Whitford-Stark and Head, 1977). It's believed that Aristarchus crater turned over the basalts and exposed KREEP-rich materials below (Gillis et al., 2004). While, evident traces of magmatism confuse the origin of radioactivity and demonstrate a potential volcanogenic source.

Limited by inherent spatial resolution of CGRS, it's difficult to distinguish these two geologic processes via radioelements distribution of Aristarchus region in our result.

Other basins (Serenitatis, Humorum, etc.) located on the edge of PKT can't be well distinguished in the radioelements maps (shown in Fig. 6). These basins forming in Pre-Imbrium Epoch (Wilhelms and McCauley, 1971) might have been contaminated by Imbrium ejecta so that we cannot determine whether there are local radioactive contribution other than Imbrium, and the same case may happen for Mare Nubium and Tranquillitatis.

3.2. SPAT

South Pole Aitken Basin (SPA), the largest impact basin of solar system, was inferred to have excavated materials in depth of lower crust, and even upper mantle (Lucey et al., 1998). Radioactive enhancements are observed within SPA (~0.4–3.39 ppm Th; see Fig. 7) compared with FHT outsides (<0.4 ppm Th), while the magnitude is just comparable to the level of PKT's edge and much less than the peak values (~11.0 ppm Th). It seems to provide another evidence for the speculation that KREEP-rich residua are concentrated in PKT. Other than magma ocean differentiation, substantial meteorite bombardments after the formation of SPA, especially during Nectarian and Lower Imbrium Epoch, would be likely to garden the surface of SPA and weaken possible higher radioactivity than observed from orbiters now.

Asymmetrical distribution of radioactive signatures can be noticed within SPA that radioactive abundances decrease along the northwest to southeast direction (~1.1–3.39 ppm Th in the northwestern portion versus ~1.1–2.27 ppm Th in the southeastern portion). Coupled with elliptical structure in topography (see Fig. 7), it suggests that the event forming SPA might be an oblique impact (Garrick-Bethell and Zuber, 2009).

Magmatic processes seem to be also related to radioactive distribution in SPA. The hot spots of radioelements are roughly corresponding to Mare Von Kármán (~3.2 ppm Th), Ingenii (~3.39 ppm Th) and several other volcanic regions in SPA as shown in Fig. 7. Like the topographic and radioactive asymmetries, majority of mare basalts concentrate in the western or northwestern portions of SPA as well, revealing that heat released by radioactivity would have promoted thermal evolution of this unique terrane.

3.3. FHT

Lunar highlands are regarded as typical representations of anorthositic crust originating from initial differentiation of the Moon (Warren, 1985). Therefore, highlands appears poverty of radioelements (majority lower than 2 ppm Th), which are difficult to be incorporated into crystal structure during the solidification of LMO (Korotev, 1998). These incompatible elements would gradually concentrated in the late-formed crust as the cooling of LMO. This scenario could lead to an inverse correlation between incompatible components and crustal thickness that have been found by previous gamma ray remote sensing (Metzger et al., 1977; Lawrence et al., 2000; Kobayashi et al., 2012). Besides protosomatic sources, Haskin et al. (1998) claimed that KREEP-bearing ejecta from Imbrium impact could contaminate as far as the surface of FHT and even SPA. The CGRS Th distribution outside of Imbrium (except SPA) decreases as the distance from center of Imbrium increases (Fig. 8) that also agrees with the hypothesis of Imbrium ejecta. Anyway, further investigations are required to examine the weight of protosomatic or enthetic sources for the radioactivity of FHT.

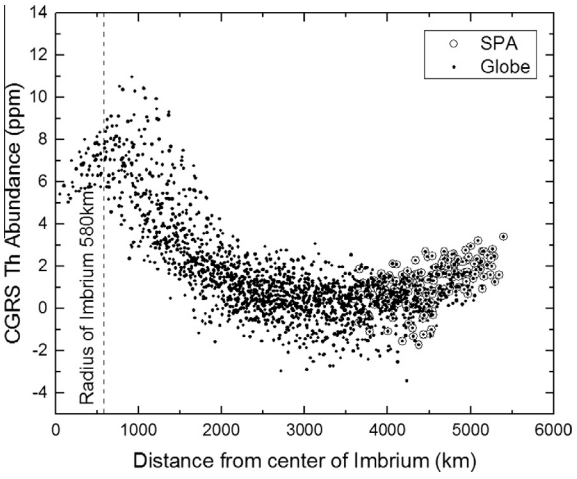

Fig. 8. Relationship between CGRS Th abundance and the distance from center of Imbrium.

4. Summary

We have acquired global concentrations of radioelements utilizing CGRS level 2C scientific data. Based on the previous CGRS studies (Zhu et al., 2010, 2011; Zou et al., 2011), and together with spectral fitting techniques, we updated the procedures of data processing with emphasis on extracting contribution of radioelements from composite peaks. Moreover, we applied a calibration model that correlates peak areas of CGRS and the ground truths from lunar samples and meteorites.

The global maps of lunar radioelements acquired by CGRS show the heterogenous distribution across lunar surface, thus help us better understand the petrogenesis in lunar terranes. The findings of an oval pattern surrounding Imbrium and Aristarchus radioactive anomaly agree well with previous studies. The CGRS radioelements maps are also in support of the nonimpact origin of Procellarum region, and our study suggests that basaltic lava flows might play a crucial role in the emplacement of KREEP materials in PKT. CGRS also confirmed the radioactive occurrence and asymmetric distribution in SPA, which could have constrained local volcanic activity. In addition, the distribution of radioelements matches well with the

view that radioactivity in FHT possibly originated from deposition of Imbrium ejecta while the contribution degree compared to protogenous inventory would need more investigations.

For future work, we will concentrate on further study of CGRS data and combine with more recently distributed lunar gamma ray datasets (e.g., Chang'E-2 and Kaguya/Selene, Kobayashi et al., 2010, 2012; Yamashita et al., 2010; Zhu et al., 2013, 2014, 2015) that would enable us better investigate the origin of lunar radioelements distribution at higher spatial and spectral resolutions.

Acknowledgment

This work was supported partially by the National Natural Science Foundation of China (41373068, 41473065, 41490634, U1231103), National Science and Technology Infrastructure Work Projects (2015FY210500), Natural Science Foundation of Shandong Province (ZR2015DQ001, JQ201511), and CAS Key Laboratory of Lunar and Deep Space Exploration through Grant. We also appreciate the three anonymous reviewers for their detailed comments and valuable suggestions.

References

Andrews-Hanna, J.C., Jonathan, B., Head, J.W., et al., 2014. Structure and evolution of the lunar Procellarum region as revealed by GRAIL gravity data. Nature 514 (7520), 68–71.

Bielefeld, M.J., Reedy, R.C., Metzger, A.E., et al., 1976. Surface chemistry of selected lunar regions. Lunar and Planetary Science Conference Proceedings. Lunar and Planetary Science Conference Proceedings, pp. 2661–2676.

Feldman, W.C., Ahola, K., Barraclough, B.L., et al., 2004. Gamma-Ray, neutron, and alpha-particle spectrometers for the lunar prospector mission. J. Geophys. Res. 109 (E7), 443–459.

Garrick-Bethell, I., Zuber, M.T., 2009. Elliptical structure of the lunar South Pole-Aitken basin. Icarus 204 (2), 399–408.

Gillis, J.J., Jolliff, B.L., Korotev, R.L., 2004. Lunar surface geochemistry: global concentrations of Th, K, and FeO as derived from lunar prospector and Clementine data. Geochim. Cosmochim. Acta 68 (18), 3791–3805.

Harrington, T.M., Marshall, J.H., Arnold, J.R., et al., 1974. The Apollo gamma-ray spectrometer. Nucl. Instrum. Methods 118 (74), 401–411.

Hasebe, N., Yamashita, N., Okudaira, O., et al., 2008. The high precision gamma-ray spectrometer for lunar polar orbiter SELENE. Adv. Space Res. 42 (2), 323–330.

Haskin, L., Warren, P., 1991. Lunar chemistry. In: Lunar Sourcebook, Cambridge University Press, vol. 4, 1991, pp. 357–474.

Haskin, L.A., Korotev, R.L., Rockow, K.M., et al., 1998. The case for an Imbrium origin of the Apollo thorium-rich impact-melt breccias. Meteorit. Planet. Sci. 33 (5), 959–975.

Haskin, L.A., Gillis, J.J., Korotev, R.L., et al., 2000. The materials of the lunar Procellarum KREEP terrane: a synthesis of data from geomorphological mapping, remote sensing, and sample analyses. J. Geophys. Res. Planets 105 (E8), 20403–20415 (1991–2012).

Jolliff, B.L., Gillis, J.J., Haskin, L.A., et al., 2000. Major lunar crustal terranes: surface expressions and crust–mantle origins. J. Geophys. Res. Planets 105 (E2), 4197–4216 (1991–2012).

Jolliff, B.L., Wieczorek, M.A., Shearer, C.K., et al., 2006. New Views of the Moon, Reviews in Mineralogy and Geochemistry, vol. 60. Mineralogical Society of America, Chantilly, VA.

Kobayashi, S., Hasebe, N., Shibamura, E., et al., 2010. Determining the absolute abundances of natural radioactive elements on the lunar surface by the Kaguya gamma-ray spectrometer. Space Sci. Rev. 154 (1–4), 193–218.

Kobayashi, S., Karouji, Y., Morota, T., et al., 2012. Lunar farside Th distribution measured by Kaguya gamma-ray spectrometer. Earth Planet. Sci. Lett. 337 (4), 10–16.

Korotev, R.L., 1998. Concentrations of radioactive elements in lunar materials. J. Geophys. Res. Planets 103 (E1), 1691–1701 (1991–2012).

Korotev, R.L., Jolliff, B.L., Zeigler, R.A., et al., 2003. Feldspathic lunar meteorites and their implications for compositional remote sensing of the lunar surface and the composition of the lunar crust. Geochim. Cosmochim. Acta 67 (24), 4895–4923.

Lawrence, D.J., Feldman, W.C., Barraclough, B.L., et al., 2000. Thorium abundances on the lunar surface. J. Geophys. Res. Planets 105 (8), 20307–20331 (1991–2012).

Lawrence, D.J., Elphic, R.C., Feldman, W.C., et al., 2003. Small-area thorium features on the lunar surface. J. Geophys. Res. 108 (E9), 369–378.

Lawrence, D.J., Maurice, S., Feldman, W.C., 2004. Gamma-ray measurements from lunar prospector: time series data reduction for the gamma-ray spectrometer. J. Geophys. Res. Planets 109 (7) (1991–2012).

Lucey, P.G., Taylor, G.J., Hawke, B., et al., 1998. FeO and TiO_2 concentrations in the South Pole-Aitken basin: implications for mantle composition and basin formation. J. Geophys. Res. Planets 103 (E2), 3701–3708 (1991–2012).

Ma, T., Chang, J., Zhang, N., et al., 2008. Gamma-ray detector on board lunar mission Chang'E-1. Adv. Space Res. 42 (2), 347–349.

Metzger, A.E., Haines, E.L., Parker, R.E., et al., 1977. Thorium concentrations in the lunar surface. I – Regional values and crustal content. Lunar and Planetary Science Conference Proceedings, pp. 949–999.

Papike, J.J., Ryder, G., Shearer, C.K., 1998. Lunar samples. Rev. Mineral. Geochem. 36 (1), 5.1-5.234.

Prettyman, T.H., Hagerty, J.J., Elphic, R.C., et al., 2006. Elemental composition of the lunar surface: analysis of gamma ray spectroscopy data from lunar prospector. J. Geophys. Res. Planets 111 (E12) (1991–2012).

Smith, D.E., Zuber, M.T., Neumann, G.A., et al., 2010. Initial observations from the lunar orbiter laser altimeter (LOLA). Geophys. Res. Lett. 37 (18).

Warren, P.H., 1985. The magma ocean concept and lunar evolution. Annu. Rev. Earth Planet. Sci. 13, 201–240.

Whitford-Stark, J.L., Head, J.W., 1977. The Procellarum volcanic complexes-contrasting styles of volcanism. Lunar and Planetary Science Conference Proceedings, vol. 8, pp. 2705–2724.

Wieczorek, M.A., Phillips, R.J., 2000. The, Procellarum KREEP terrane: implications for mare volcanism and lunar evolution. J. Geophys. Res. Planets 105 (E8), 20417–20430 (1991–2012).

Wieczorek, M.A., Neumann, G.A., Nimmo, F., et al., 2013. The crust of the Moon as seen by GRAIL. Science 339 (6120), 671–675.

Wilhelms, D.E., McCauley, J.F., 1971. Geologic Map of the Near Side of the Moon, US Geological Survey, Reston.

Wilhelms, D.E., McCauley, J.F., Trask, N.J., 1987. The Geologic History of the Moon. Washington: USGPO; Denver, CO (Federal Center, Box 25425, Denver 80225): For Sale by the Books and Open-file Reports Section, US Geological Survey, 1.

Yamashita, N., Hasebe, N., Reedy, R.C., et al., 2010. Uranium on the Moon: global distribution and U/Th ratio. Geophys. Res. Lett. 37 (10), 198–209.

Zhang, L.Y., Zou, Y.L., Liu, J.Z., et al., 2011. Time series data correction for the Chang'E-1 gamma-ray spectrometer. Res. Astron. Astrophys. 11 (6), 737.

Zhu, M.H., Ma, T., Chang, J., 2010. Chang'E-1 gamma ray spectrometer and preliminary radioactive results on the lunar surface. Planet. Space Sci. 58 (12), 1547–1554.

Zhu, M.H., Ma, T., Chang, J., et al., 2011. Lunar potassium distribution: results from Chang'E-1 gamma ray spectrometer. Sci. China Phys. Mech. Astron. 54 (11), 2083–2090.

Zhu, M.H., Chang, J., Ma, T., et al., 2013. Potassium map from Chang'E-2 constraints the impact of Crisium and Orientale basin on the Moon. Sci. Rep. 3, 1611-1611.

Zhu, M.H., Chang, J., Fa, W.Z., et al., 2014. Thorium on the lunar highlands surface: insights from Chang'e-2 gamma-ray spectrometer. Lunar and Planetary Science Conference, vol. 45, pp. 1237.

Zhu, M.H., Chang, J., Xie, M., et al., 2015. The uniform K distribution of the mare deposits in the Orientale Basin: Insights from Chang'E-2 gamma-ray spectrometer. Earth Planet. Sci. Lett. 418, 172–180.

Zou, Y., Zhang, L., Liu, J., et al., 2011. Data analysis of Chang'E-1 gamma-ray spectrometer and global distribution of U, K, and Th elemental abundances. Acta Geol. Sin. 85 (6), 1299–1309.